



# CHORUS

This is the accepted manuscript made available via CHORUS. The article has been published as:

## Labyrinthine domains in ferroelectric nanoparticles: Manifestation of a gradient-induced morphological transition

Eugene A. Eliseev, Yevhen M. Fomichov, Sergei V. Kalinin, Yulian M. Vysochanskii, Peter Maksymovich, and Anna N. Morozovska

Phys. Rev. B **98**, 054101 — Published 2 August 2018

DOI: [10.1103/PhysRevB.98.054101](https://doi.org/10.1103/PhysRevB.98.054101)

# **Labyrinthine domains in ferroelectric nanoparticles: a manifestation of gradient-induced morphological transition**

*Eugene A. Eliseev<sup>1</sup>, Yevhen M. Fomichov<sup>1</sup>, Sergei V. Kalinin<sup>2</sup>, Yulian M. Vysochanski<sup>3</sup>, Peter Maksymovich<sup>2</sup> and Anna N. Morozovska<sup>4,5\*</sup>*

<sup>1</sup> *Institute for Problems of Materials Science, National Academy of Sciences of Ukraine,  
Krjijanovskogo 3, 03142 Kyiv, Ukraine*

<sup>2</sup> *The Center for Nanophase Materials Sciences, Oak Ridge National Laboratory,  
Oak Ridge, TN 37831*

<sup>3</sup> *Institute of Solid State Physics and Chemistry, Uzhgorod University,  
88000 Uzhgorod, Ukraine*

<sup>4</sup> *Institute of Physics, National Academy of Sciences of Ukraine,  
46, pr. Nauky, 03028 Kyiv, Ukraine*

<sup>5</sup> *Bogolyubov Institute for Theoretical Physics, National Academy of Sciences of Ukraine,  
14-b Metrolohichna str. 03680 Kyiv, Ukraine*

## **Abstract**

In the framework of the Landau-Ginzburg-Devonshire (LGD) approach we studied finite size effects of the phase diagram and domain structure evolution in spherical nanoparticles of uniaxial ferroelectric. The particle surface is covered by a layer of screening charge characterized by finite screening length. The phase diagram, calculated in coordinates "particle radius – screening length" has a wide region of versatile poly-domain structures separating single-domain ferroelectric and nonpolar paraelectric phases. Unexpectedly, we revealed a region of irregular labyrinthine domains in the nanoparticles of uniaxial ferroelectric  $\text{CuInP}_2\text{S}_6$  with the first order paraelectric-ferroelectric phase transition. We established that the origin of labyrinthine domains is the mutual balance of LGD, polarization gradient and electrostatic energies. The branching of the domain walls appears and increases rapidly when the polarization gradient energy decreases below the critical value. Allowing for the generality of LGD approach, we expect that the gradient-induced morphological transition can be the source of labyrinthine domains appearance in many spatially-confined ferroics with long-range order parameter, including relaxors, ferromagnetics, antiferrodistortive materials and materials with incommensurate ferroic phases.

---

\* corresponding author, e-mail: [anna.n.morozovska@gmail.com](mailto:anna.n.morozovska@gmail.com)

## I. INTRODUCTION

The ferroic materials described by Landau theory of symmetry-breaking have a substantial impact on fundamental science and various applications. Different types of topological defects in different ferroics (ferromagnets, ferroelectrics, ferroelastics) are even more numerous and enigmatic than different types of symmetry-breaking, and consequently, they become one of the key fundamental problems and hot topics in scientific community [1, 2].

Complementary to the topological point defects [1], domain walls can be considered as extended 2D topological defects in ferroics (see e.g. chapter 8 in [2] and refs. therein). Vortices and vertices composed by the closure of four domain walls have been observed experimentally and described theoretically in a bulk and nanosized ferroelectrics [3, 4, 5, 6, 7]. Stable surface-induced labyrinthine domain structures were observed by Piezoresponse Force Microscopy (PFM) in ergodic ferroelectrics relaxors and explained by the presence of higher-order term in free-energy expansion that gives rise to the polarization modulations [8]. Fractal domain structures are sometimes observed in multiferroic thin films [9] and near the surface of relaxors close to relaxor-ferroelectric boundary [10], but the labyrinthine domains with a single characteristic length scale were observed by PFM in ergodic relaxors only [8]. These labyrinthine structures can coexist with classical ferroelectric domains closer to ferroelectric composition limit [11, 12]. The labyrinthine domain structure was predicted theoretically in thin films of incommensurate ferroelectrics [13] and bi-layered ferroelectrics [14], being similar to those observed in ultrathin magnetic films [15].

However, we did not find any experimental observation or theoretical prediction of labyrinthine domains in the nanoparticles of ordered ferroelectrics, which intriguing polar and dielectric properties attract permanent attention of researchers. Classical examples are unexpected experimental results of Yadlovker and Berger [16, 17, 18], which reveal the enhancement of polar properties of cylindrical nanoparticles of Rochelle salt. Frey and Payne [19], Zhao et al [20], Droblich et al [21], Erdem et al [22] and Golovina et al [23, 24, 25] demonstrate the possibility to control the phase transitions (including new polar phases appearance) for  $\text{BaTiO}_3$ ,  $\text{S}_2\text{P}_2\text{S}_6$ ,  $\text{PbTiO}_3$  and  $\text{KTa}_{1-x}\text{Nb}_x\text{O}_3$  nanopowders and nanoceramics by **finite size effects**.

The theory of finite size effects in nanoparticles allows one to establish the physical origin of the polar and dielectric properties anomalies, and phase diagrams changes appeared under the nanoparticles sizes decrease. In particular, using the continual phenomenological approach Niepce [26], Huang et al [27, 28], Ma [29], Eliseev et al [30] and Morozovska et al [31, 32, 33] have shown, that the changes of the transition temperatures, the enhancement or weakening of polar properties in a **single-domain** spherical and cylindrical nanoparticles are conditioned by the various physical mechanisms, such as correlation effect, depolarization field, flexoelectricity, electrostriction, surface tension and Vegard-type chemical pressure.

Notably depolarization field always decreases ferroelectric polarization and transition temperature, especially under the presence of imperfect screening [34, 35, 36]. For majority of models the particles were regarded covered with perfect electrodes and so their single-domain state would be stable. Only few models describing the imperfect screening effect in nanoparticles have been evolved [34-36].

To fill the gap in the knowledge, below we analyze the phase diagram and domain structure evolution in spherical nanoparticles of uniaxial ferroelectric  $\text{CuInP}_2\text{S}_6$  (**CIPS**). We regarded that the particle surface is covered by a layer of screening charge characterized by finite screening length. The imperfect screening and finite size effects are studied using the Landau-Ginzburg-Devonshire (**LGD**) approach combined with the electrostatic equations. We revealed that a regular stripe domain structure avalanche-like transforms into a labyrinth pattern with a gradient term decrease below the critical value and classified the event as a **gradient-induced** morphological transition.

The applicability of LGD approach for thin films and nanoparticles with radius less than (2-10) nm is corroborated by the fact, that the critical sizes of the long-range order appearance and properties calculated from atomistic [37, 38, 39, 40, 41] and phenomenological [30-33, 42, 43] theories are in a good agreement with each other as well as with experimental results for nanosized ferromagnetics [44] and ferroelectrics [16-20, 22, 45]. Both atomistic simulations and LGD-description are absent for CIPS nanoparticles.

## II. THEORETICAL APPROACH

Let us consider a CIPS nanoparticle of radius  $R$  with a one-component ferroelectric polarization  $P_3(\mathbf{r})$  directed along the crystallographic axis 3 [**Fig.1(a)**]. The particles are covered by a layer of screening charge with a surface charge density  $\sigma$  characterized by a nonzero screening length  $\lambda$ . The specific nature of the surface charge can be, e.g., Bardeen-type surface states [46]. For the case the screening charges can be localized at surface states caused by the strong band-bending via depolarization field [47, 48, 49, 50, 51], at that  $\lambda$  can be much smaller ( $\leq 0.1$  nm) than a lattice constant ( $\sim 0.5$  nm) [34]. Concrete expression for  $\lambda$  can be derived in, e.g., Stephenson-Highland ionic adsorption model [52, 53, 54], by the linearization of  $\sigma$ , as  $\sigma \approx -\epsilon_0 \phi/\lambda$ , where

$$\lambda^{-1} \approx \sum_i \frac{(eZ_i)^2}{4\epsilon_0 A_i k_B T} \left( 1 - \tanh^2 \left( \frac{\Delta G_i^{00}}{2k_B T} \right) \right),$$

$Z_i$  is the ionization number of the surface ions,  $1/A_i$  is their saturation densities,  $\Delta G_i^{00}$  is the free energy of the surface ion formation,  $\epsilon_0$  is a universal dielectric constant. In general case  $\lambda$  depends on temperature  $T$  and screening charges nature. Since we do not know the temperature dependence of  $\lambda$ , we performed calculations regarding  $\lambda$  changing in the range  $(10^{-3} - 1)$  nm.

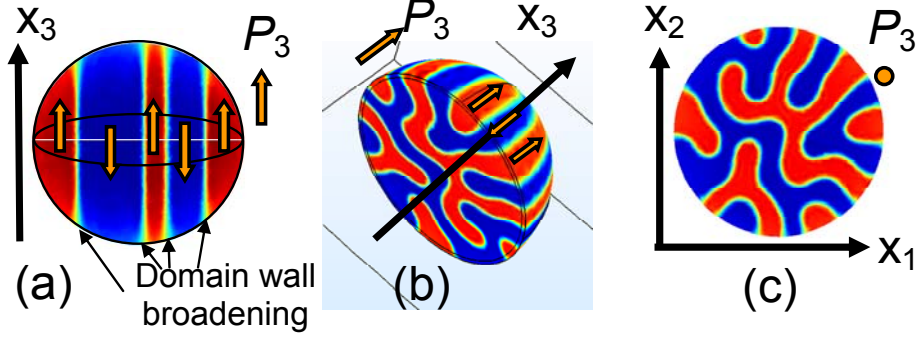


**FIG. 1.** Labyrinthine domains in a spherical CIPS nanoparticle. (a) Polar cross-section, (b) semi-spherical view and (c) equatorial cross-section. Radius  $R=10$  nm, screening length  $\lambda=0.03$  nm, room temperature 293 K. CIPS parameters are listed in **Table I**.

For a layered perovskite with layers plane (001) and ferroelectric dipoles directed in the out-of-plane direction, we can assume that the dependence of the in-plane components of electric polarization on the inner field electric  $E_i$  is linear  $P_i = \epsilon_0(\epsilon_b - 1)E_i$  ( $i = 1, 2$ ), where an isotropic background permittivity  $\epsilon_b$  is relatively small,  $\epsilon_b \leq 10$  [55]. Polarization component  $P_3(\mathbf{r})$  contains background and soft mode contributions. Electric displacement vector has the form  $\mathbf{D} = \epsilon_0\epsilon_b\mathbf{E} + \mathbf{P}$  inside the particle and  $\mathbf{D} = \epsilon_0\epsilon_e\mathbf{E}$  outside it;  $\epsilon_e$  is the relative dielectric permittivity of external media regarded unity (air or vacuum).

Euler-Lagrange equation for the ferroelectric polarization  $P_3(\mathbf{r})$  follows from the minimization of LGD free energy functional  $G = G_{Landau} + G_{grad} + G_{el} + G_{es+flexo}$ , that includes Landau expansion,  $G_{Landau}$ , polarization gradient energy contribution,  $G_{grad}$ , electrostatic contribution  $G_{el}$ , and elastic, electrostriction and flexoelectric contributions  $G_{es+flexo}$  (see e.g. [30, 35, 56]):

$$G_{Landau} = \int_{|\vec{r}| < R} d^3r \left( \frac{\alpha}{2} P_3^2 + \frac{\beta}{4} P_3^4 + \frac{\gamma}{6} P_3^6 \right), \quad (1a)$$

$$G_{grad} = \int_{|\vec{r}| < R} d^3r \left( \frac{g_{11}}{2} \left( \frac{\partial P_3}{\partial x_3} \right)^2 + \frac{g_{44}}{2} \left[ \left( \frac{\partial P_3}{\partial x_2} \right)^2 + \left( \frac{\partial P_3}{\partial x_1} \right)^2 \right] \right), \quad (1b)$$

$$G_{el} = - \int_{|\vec{r}| < R} d^3r \left( P_3 E_3 + \frac{\epsilon_0 \epsilon_b}{2} E_i E_i \right) - \int_{|\vec{r}| = R} d^2r \left( \frac{\epsilon_0 \Phi^2}{2\lambda} \right) - \frac{\epsilon_0 \epsilon_e}{2} \int_{|\vec{r}| > R} E_i E_i d^3r, \quad (1c)$$

$$G_{es+flexo} = \int_{|\vec{r}| < R} d^3r \left( - \frac{S_{ijkl}}{2} \sigma_{ij} \sigma_{kl} - Q_{ij3} \sigma_{ij} P_3^2 - F_{ijk3} \left( \sigma_{ij} \frac{\partial P_3}{\partial x_k} - P_3 \frac{\partial \sigma_{ij}}{\partial x_k} \right) \right). \quad (1d)$$

Here  $E_i$  are electric field components related with electric potential  $\phi$  as  $E_i = -\partial\phi/\partial x_i$ . The coefficient  $\alpha$  linearly depends on temperature  $T$ ,  $\alpha = \alpha_T(T - T_C)$ , where  $T_C$  is the Curie temperature. The coefficient  $\beta$  is temperature-independent and negative, since CIPS undergoes the first order transition to paraelectric phase. Coefficient  $\gamma$  and gradient coefficients  $g_{11}$  and  $g_{44}$  are positive and temperature independent. An isotropic approximation,  $g_{44} \approx g_{55}$  in (001) plane was taken for monoclinic CIPS structure.  $\sigma_{ij}$  is the stress tensor in Eq.(1d). We omit the evident form of the  $G_{es+flexo}$  for the sake of simplicity, it is listed in Refs.[57, 58, 59]. Since the values of the electrostriction and flexoelectric tensor components,  $Q_{ijkl}$  and  $F_{ijkl}$ , are unknown for CIPS, we performed numerical calculations using finite element method (**FEM**) with the coefficients varied in a physically reasonable range ( $|F_{ijkl}| \leq 10^{11} \text{ m}^3/\text{C}$  and  $|Q_{ijkl}| \leq 0.1 \text{ m}^4/\text{C}^2$ ). Results proved the insignificant impact of electrostriction and flexoelectric coupling on domain morphology [60]. Other LGD parameters for a bulk ferroelectric CIPS were taken from Ref.[61] and are listed in **Table I**.

**Table I.** LGD parameters for bulk ferroelectric  $\text{CuInP}_2\text{S}_6$ , used in calculations

$\epsilon_b$	$\alpha_T(\text{C}^{-2} \cdot \text{m J/K})$	$T_C(\text{K})$	$\beta(\text{C}^{-4} \cdot \text{m}^5 \text{J})$	$\gamma(\text{C}^{-6} \cdot \text{m}^9 \text{J})$	$g_{11}(\text{m}^3/\text{F})$ [62]	$g_{44}(\text{m}^3/\text{F})$
7	$1.569 \times 10^7$	302	$-1.8 \times 10^{12}$	$2.2 \times 10^{15}$	$1.0 \times 10^{-10}$	vary in the range $(0.3 - 3) \times 10^{-11}$

Allowing for Khalatnikov mechanism of polarization relaxation, corresponding Euler-Lagrange equation for  $P(\mathbf{r}_3)$  becomes time-dependent LGD-equation [63]:

$$\Gamma \frac{\partial P_3}{\partial t} + \alpha(T)P_3 + \beta P_3^3 + \gamma P_3^5 - g_{44} \left( \frac{\partial^2}{\partial x_1^2} + \frac{\partial^2}{\partial x_2^2} \right) P_3 - g_{11} \frac{\partial^2 P_3}{\partial x_3^2} = E_3. \quad (2)$$

The Khalatnikov coefficient  $\Gamma$  determines the relaxation time of polarization  $\tau_K = \Gamma/|\alpha|$ , that typically varies in the range  $(10^{-11} - 10^{-13})\text{s}$  far from  $T_C$ . The boundary condition for  $P$  at the spherical surface is natural,  $\partial \bar{P} / \partial \mathbf{n} \big|_{r=R} = 0$ ,  $\mathbf{n}$  is the outer normal to the surface.

Electric potential  $\phi$  satisfies a Poisson equation inside the particle,

$$\epsilon_0 \epsilon_b \Delta \phi = -\frac{\partial P}{\partial x_3}, \quad (3a)$$

and Laplace equation outside it,

$$\Delta \phi = 0. \quad (3b)$$

3-D Laplace operator is denoted by the symbol  $\Delta$ . Equations (3) are supplemented by the condition of potential continuity at the particle surface,  $(\phi_{ext} - \phi_{int}) \big|_{r=R} = 0$ . The boundary condition for the

normal components of electric displacements,  $(\mathbf{n}(\mathbf{D}_{ext} - \mathbf{D}_{int}) + \sigma)|_{r=R} = 0$ , where the surface charge density  $\sigma = -\epsilon_0 \phi/\lambda$ .

In fact the screening length  $\lambda$  decrease improves the screening conditions, which leads to a decrease in the depolarization field and hence and the domains eventual disappear giving way to a more energetically favorable single-domain state (see e.g. Fig.2 in Ref.[58]).

### III. NUMERICAL RESULTS AND DISCUSSION

#### A. Main features of phase diagrams at different temperatures

Phase diagrams was studied at different temperatures in the range (300 – 200) K. Unfortunately we do not know the temperature dependence of  $\lambda$ , and so we perform all calculations regarding  $\lambda$  changing in the range ( $10^{-3} - 1$ ) nm. Phase diagram of CIPS nanoparticles calculated at T=293 K and 200 K in coordinates "radius  $R$  – screening length  $\lambda$ " is shown in **Fig. 2(a)** and **2(b)**, respectively.

At room temperature the phase diagram has an unexpectedly wide region of stable poly-domain states (**PDFE**) separating single-domain ferroelectric (**SDFE**) and nonpolar paraelectric (**PE**) phases [see **Fig. 2(a)**]. The bottom row shows the typical changes of polarization distribution in the equatorial cross-section of the nanoparticle with  $R=5$  nm, which happens with increase of  $\lambda$ . A single-domain state is stable at very small  $\lambda < 0.01$  nm, two-domain structure (electric quadrupole) is stable in the interval  $0.01 < \lambda < 0.017$  nm, three-domain structure (electric octupole) exist at  $0.017 < \lambda < 0.019$  nm, 2N-multipolar domain stripes are stable at  $0.02 < \lambda < 0.035$  nm. Coexistence of PDFE and PE phase when the nanoparticle consists of PE surface layer and ferroelectric domain stripes in the core appears at  $0.035 < \lambda < 0.045$  nm, and is followed by the size-induced phase transition into a stable PE at  $\lambda > 0.045$  nm. Unexpectedly, we revealed a region of stable "labyrinthine" domains (**LD**) of irregular shape (yellow circles) inside the region of regular domain structures with quadruple two (purple circles) or multiple (magenta circles) domain stripes. LD region is within a dashed parallelogram in **Fig.2(a)**. We should underline, that LD stability (or more rigorously speaking "long-living" metastabilty) does not mean their **absolute stability**, because we cannot make a sweep over all possible domain configurations to choose the one or several equivalent ones, which energy reaches an absolute minimum.

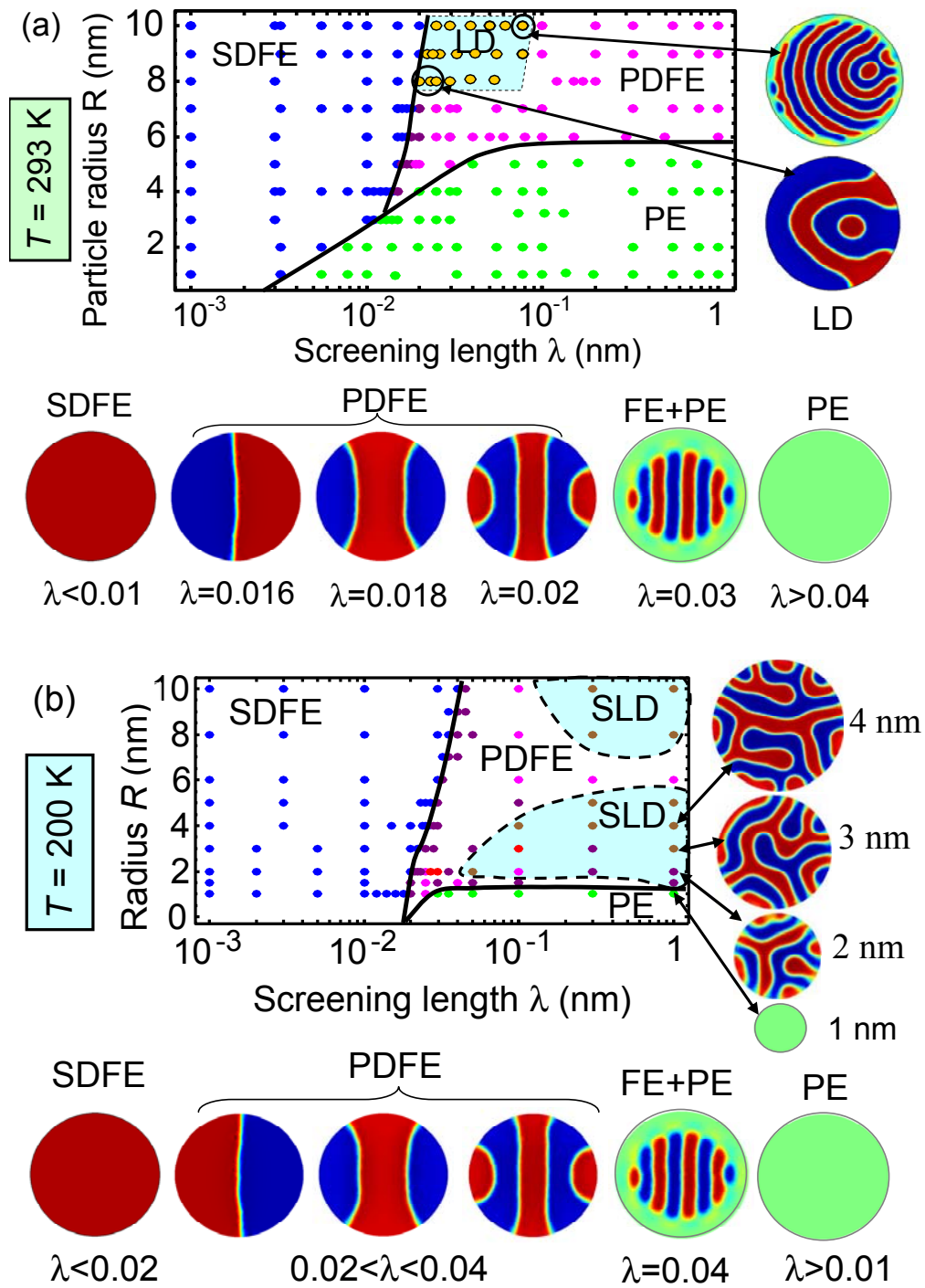


**FIG. 2.** Phase diagram of CIPS nanoparticles in coordinates "radius  $R$  – screening length  $\lambda$ " calculated for the gradient coefficient  $g_{44}=2 \times 10^{-11} \text{ m}^3/\text{F}$  and temperatures 293 K (a) and 200 K (b). The ferroelectric single domain (SDFE), ferroelectric poly domain (PDFE) and paraelectric (PE) phases are shown by different colors of the circles. The labyrinthine domains (LD) are located within dashed light-blue regions. The bottom rows shows typical polarization distributions in the equatorial cross-sections of the nanoparticles with radius  $R=5 \text{ nm}$  and different values of  $\lambda$  (in nm). CIPS parameters are listed in **Table I**.



With the temperature decrease from 293 K (that is very close to the CIPS Curie temperature 302 K) to 200 K the region of a SDFE significantly increases towards smaller radii  $R$  (up to the very small  $R=1$  nm for which LGD applicability becomes questionable) and higher  $\lambda$  (from e.g.  $\lambda=0.003$  nm at 293 K to 0.02 nm at 200 K) [compare the size of SDFE regions in **Fig.2(a)** and **2(b)**]. The wide region of PE phase (present at 293 K) almost disappears with the temperature decreasing to 200 K leading to the conclusion that PDFE state can be stable in ultra-small CIPS nanoparticles (with radius less than 2 nm) covered by a screening charge [compare the size of PE regions in **Fig.2(a)** and **2(b)**]. The shift and increase of LD region(s) are evident with the temperature decrease from 300 to 200 K [compare the size and positions of LD regions in **Fig.2(a)** and **2(b)**]. The increase of SDFE, PDFE and LD regions with the temperature  $T$  decrease stem from the well-established fact that FE phase becomes deeper and wider with the temperature increase, since the coefficient  $\alpha = \alpha_T(T - T_C)$  acquires higher negative values with  $T$  decrease below Curie temperature  $T_C$ .

The effect of geometric catastrophe can be imagined from the images of LD in the nanoparticles of radius 4, 3 and 2 nm for which the number of branches and sharp bendings of domain walls gradually decreases with the particle radius decrease from 4 nm to 2 nm [see right column in **Fig. 2(b)**]. Eventually LD disappears for  $R=1$  nm. Hence the effect of geometric catastrophe suppresses the LD in small particles.

Note the validity of our prediction regarding LD appearance and PDFE state conservation for nanoparticles of sizes more than  $2R = 4$  nm, because they corresponds to 10 lattice constants or more. It is general opinion that LGD approach can be valid only qualitatively for the sizes less than 10 *l.c.* [16-20, 22, 30-33], and must be approved by *ab initio* calculations.

## B. Labyrinthine domains stability and evolution

Polarization distributions in the equatorial cross-section of the nanoparticle with radius  $R=10$  nm, screening length  $\lambda=0.03$  nm and room temperature are shown in **Fig. 3**. Top row shows initial seedings of the distributions shown in the lower row. The energy values computed for the single-domain [**Fig.3(a)**], two-domain [**Fig.3(b)**], three-domain [**Fig.3(c)**], axially-symmetric domains [**Fig.3(d)**], eight-domain stripes [**Fig.3(e)**] and the labyrinthine domain structure [**Fig.3(f)**] are  $G = -5.98, -6.94, -7.08, -8.50, -8.55$  and  $-9.04$  (in  $10^{-20}$  J) at fixed value of  $g_{44}=2 \times 10^{-11}$  m<sup>3</sup>/F. Thus the ‘‘labyrinthine’’ structure has the minimal energy corresponding the optimal balance between the gradient-correlation energy (1b) tending to minimize the area of the domain walls (and hence to decrease the number of them) and electrostatic energy (1c) decreasing with domain width decrease. Note that the walls of LD are uncharged in the central part of the particle and become charged and

broadened near its poles (see yellow-blue regions near the poles in **Figs. 1(a)** and **Fig. S2** in Ref.[60]), since their broadening causes the depolarization field decrease [64].

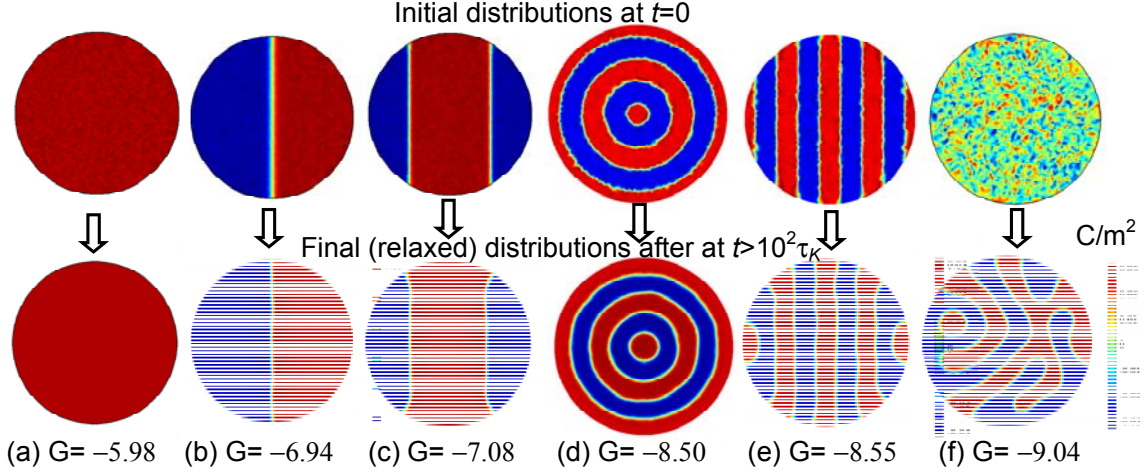


**FIG. 3.** Polarization distributions in the equatorial cross-section of the nanoparticle with  $R=10$  nm,  $\lambda=0.03$  nm,  $g_{44}=2 \times 10^{-11}$  m<sup>3</sup>/F and room temperature 293 K. Cross-sections (a)-(f) correspond to different morphologies of the domain structure, namely single-domain state (a), two-domain (b), three-domain (c), axially-symmetric domains (d), multiple stripe domains (e), and labyrinthine domains (f). Top row shows initial seedings of the distributions shown in the lower row. The scale bar is for polarization  $P_3$  in C/m<sup>2</sup>. Values of the free energy  $G$  are listed below in  $10^{-20}$  J. CIPS parameters are listed in **Table I**.

Since the problem (2)-(3) together with boundary conditions is axially symmetric (about  $x_3$  axis), one should try to find a solution with the same axial symmetry. Actually, before we "stumble" into LD and / or curved domain stripes, we specified the initial distribution of the domain structure in the form of axially symmetric distributions, e.g. in the form of coaxial cylinders shown in the top row of **Fig.3(d)**. Appeared that all radial structures are less stable than the stripes or irregular (labyrinth-like) structures [e.g. compare the energies of the final states in **Fig.3(d)**, (e) and (f)]. Radial distributions can relax to more stable distributions, and the relaxation rate depends on temperature, particle size and surface screening length. To understand why the radial domain structure in the form of coaxial cylinders has higher energy than the stripes or LD, one can use simple geometric considerations showing that when all other conditions are equal (e.g. at the same distance between the domain walls), the radial domain structure has higher surface energy than the stripes or labyrinthine structures.

An example of labyrinthine domains evolution with increase of the gradient coefficient  $g_{44}$  is illustrated in **Fig.4(a)-(e)**. Stable (in comparison with all other simulated domain structures) labyrinths exist at  $g_{44}$  less than the critical value  $g_{cr} \approx 2.5 \times 10^{-11}$  m<sup>3</sup>/F [**Fig. 4(a)-(e)**], then they transform into quasi-regular domain stripes [**Fig. 4(f)**], which in turn disappears with  $g_{44}$  increase

more than  $2.75 \times 10^{-11} \text{ m}^3/\text{F}$  [**Fig. 4(g)**]. Complementary we made sampling over 5 – 20 different labyrinthine domain patterns for each  $g_{44}$ ,  $R$  and  $\lambda$  values, which emerged with computation time from different initial random distributions of polarization inside the particle (see **Fig. S1** in Ref.[60]). From **Fig.S1** we concluded the branching number  $\Sigma$ , defined as the total number of branched domain walls, dangling branches, separated stripes and loops, decreases sharply with  $g_{44}$  increase.  $\Sigma$  varies slightly for different samples far from the critical value  $g_{cr}$  (top lines in **Fig.S1**), but the variation becomes bigger near the critical value  $g_{cr}$  (bottom lines in **Fig.S1**).

Examples of  $\Sigma$  calculation are shown in **Figs.5**. A color image of complex labyrinthine pattern with dangling branches, branch seedings, separated island and separated curved stripe is shown in **Fig.5(a)**. **Fig.5(b)** shows the black domains with white walls corresponding to the structure **(a)**. Graphs **(c, d)** with numbered features have been drawn allowing for the connectivity between different domains and particle surface in plot **5(b)**. Proposed algorithm of  $\Sigma$  calculation counts all branching points, dangling branches and separated stripes ends, which do not cross the particle from one surface to another one. Meanwhile the straight or slightly curved stripes (even very small) that cross the particle from one surface to another one do not contribute to  $\Sigma$ . However the algorithm is not ideal, because the criteria distinguishing "slightly curved" and "strongly curved" stripes are somehow voluntary. Actually, for some complex cases, like the one shown in **Fig.5(a)**, visual recalculation of  $\Sigma$  lead to different results for peculiarities number corresponding to "red" ( $\Sigma_r=7$ ) and "blue" ( $\Sigma_b=9$ ) domains [compare **Fig. 5(b)** and **5(c)**]. To improve the situation we operate with the values averaged for "red" and "blue" domains, e.g.  $\Sigma = 8$  corresponds to **Fig.5(a)**.

Graph **Fig.5 (e)** has no relation to plot **(a)**, but it is characteristic for the simpler domain patterns close the transition to LD, where the accuracy in  $\Sigma$  calculation is the most important to establish the critical value  $g_{cr}$  correctly [compare **Fig.5 (e)** with **Fig.4 (e)**]. **Fig.5(e)** illustrates how the branching point (number 5), dangling branches (numbers 1 and 2), and separated stripe ends (numbers 3 and 4), which do not cross the particle from one surface to another one, contribute to  $\Sigma$  number. Other four slightly curved stripes, which both ends at particle surfaces are marked with asterisks "\*", do not contribute to  $\Sigma$  number.

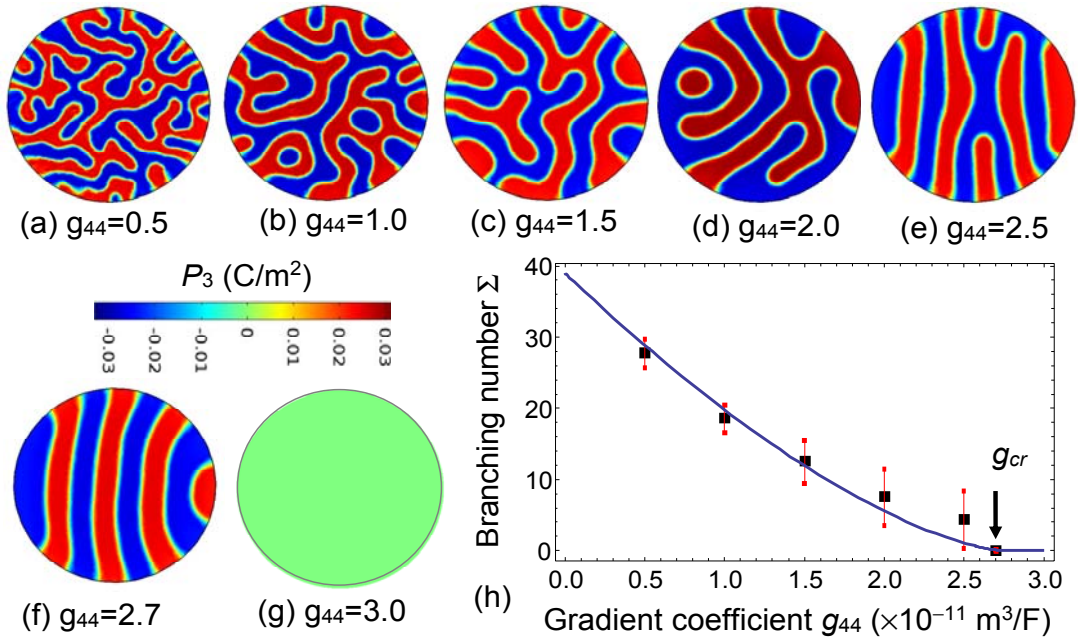


**FIG. 4.** Evolution of labyrinthine domain structure in a CIPS nanoparticle with increase of the gradient coefficient  $g_{44}$  (in  $10^{-11} m^3/F$ ) [plots (a)-(g)] for the screening length  $\lambda=0.03$  nm, radius  $R=10$  nm and room temperature 293 K. The scale bar is polarization value in  $C/m^2$ . (h) Dependence of the LD branching number  $\Sigma$  on  $g_{44}$ . Error bars corresponds to different samples of LD emerging from different initial seeding. Black circles are averaged value  $\langle \Sigma \rangle$  approximated by the function  $\langle \Sigma \rangle = 39(1 - g_{44}/g_{cr})^{3/2}$  with  $g_{cr} = 2.75 \times 10^{-11} m^3/F$  (blue curve). CIPS parameters are listed in **Table I**.

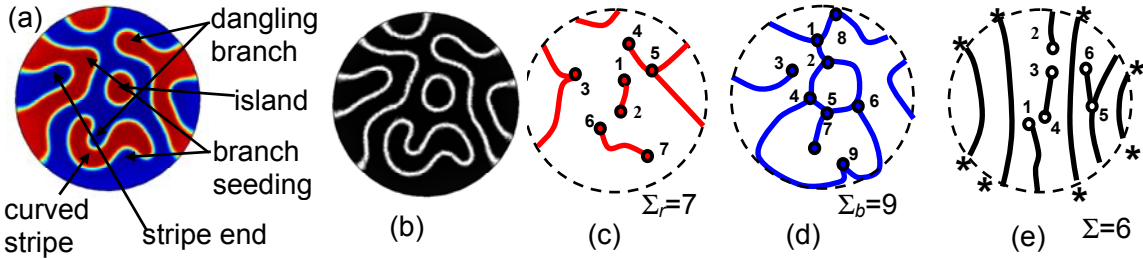


**FIG. 5. Examples of  $\Sigma$  calculation using graph method.** (a) A color image of complex labyrinthine pattern with dangling branch, branch seeding, separated island and separated curved stripe. (b) Black domains with white walls corresponding to the structure (a). Graphs (c, d) with numbered features have been drawn allowing for the connectivity between different domains and particle surface in plot (b). Graph (e) has no relation to plot (a), but it is characteristic for the patterns near the transition to LD [compare **Fig.5 (e)** with **Fig.4 (e)**].

The sampling-averaged value  $\langle \Sigma \rangle$  is not integer for fixed  $g_{44}$ . From **Fig.4(h)**, the dependence of  $\langle \Sigma \rangle$  on the gradient term  $g_{44}$  is described by the function  $\langle \Sigma \rangle = 39(1 - g_{44}/g_{cr})^{3/2}$ , and so it

continuously appears at  $g_{44} = g_{cr}$ . Hence we can associate  $\langle \Sigma \rangle$  appearance with a rapid change of the domain walls connectivity.

We leave for further studies answer on the question how the threshold of labyrinthine domain appearance and the ranges of their stability at phase diagram can be derived analytically.

The theoretical prediction of labyrinthine domains requires urgent verification by PFM, that is an ideal tool for 3D visualization of the domain structure with nanoscale resolution (see e.g. [8, 65, 66, 67, 68] and refs therein). We are convinced by a numerical calculation that qualitatively similar LD can be realized in other incompletely screened uniaxial ferroelectric nanoparticles, such as  $\text{Sn}_2\text{P}_2(\text{S},\text{Se})_6$  and  $\text{LiNbO}_3$ , with the sizes near the first-order PE-FE transition. Notably the phase diagrams in **Figs.2** can change drastically for  $\beta \geq 0$  corresponding to the second order PE-FE transition. Much more complex situation (corresponding to the balance of labyrinthine domains in the bulk and vortices at the surface) are expected in multiaxial ferroelectric nanoparticles with polarization rotation allowed, such as  $\text{BaTiO}_3$ ,  $\text{BiFeO}_3$ , however we leave a discussion of these results for further studies.

#### IV. CONCLUSION

In the framework of LGD approach combined with the equations of electrostatics, we studied the finite size effects of the phase diagrams and domain structure in spherical ferroelectric nanoparticles covered by a layer of a screening charge with finite screening length. The phase diagrams, calculated in coordinates "particle radius – screening length", has a wide region of versatile poly-domain states separating single-domain ferroelectric and nonpolar paraelectric phases. Quite unexpectedly we revealed that a regular stripe domain structure sharply transforms into a labyrinth pattern with a gradient term decrease below the critical value and named the event as a gradient-driven transition. Obtained results calculated for  $\text{CuInP}_2\text{S}_6$  can be readily generalized for other incompletely screened nanoparticles of uniaxial ferroelectrics with the first order transition to the paraelectric phase.

**Acknowledgements.** S.V.K. and P.M. study was supported by the U.S. DOE, Office of Basic Energy Sciences (BES), Materials Sciences and Engineering Division (MSED) under FWP Grant No DEAC0500OR22725. A portion of this research was conducted at the Center for Nanophase Materials Sciences, which is a DOE Office of Science User Facility. A.N.M. work was partially supported by the National Academy of Sciences of Ukraine (project No. 0118U003375 and No. 0117U002612) and by the Program of Fundamental Research of the Department of Physics and Astronomy of the National Academy of Sciences of Ukraine (project No. 0117U000240).

**Authors' contribution.** E.A.E. wrote the codes, performed numerical calculations and prepared figures. Y.M.F. tested the codes and assisted E.A.E. with simulations. A.N.M. generated research idea, stated the problem, interpreted results and wrote the manuscript. S.V.K., Y.M.V. and P.M. worked on the results discussion and manuscript improvement.

## REFERENCES

- 
- [1] N. D. Mermin, The topological theory of defects in ordered media, *Rev. Mod. Phys.* 51, 591 (1979)
- [2] *Topological Structures in Ferroic Materials*. Edited by J. Seidel, Springer Series in Mater. Sci. 228, 181 (2016).
- [3] A. Gruverman, D. Wu, H-J Fan, I Vrejoiu, M Alexe, R J Harrison and J F Scott, Vortex ferroelectric domains, *J. Phys.: Condens. Matter* 20, 342201 (2008).
- [4] N. Balke, B. Winchester, Wei Ren, Ying Hao Chu, A. N. Morozovska, E. A. Eliseev, M. Huijben, R. K. Vasudevan, P. Maksymovych, J. Britson, S. Jesse, I. Kornev, R. Ramesh, L. Bellaiche, L.-Q. Chen, and S. V. Kalinin, Enhanced electric conductivity at ferroelectric vortex cores in BiFeO<sub>3</sub>, *Nat. Phys.* 8, 81 (2012).
- [5] B. Winchester, N. Balke, X. X. Cheng, A. N. Morozovska, S. Kalinin, and L. Q. Chen, Electroelastic fields in artificially created vortex cores in epitaxial BiFeO<sub>3</sub> thin films, *Appl. Phys. Lett.* 107, 052903 (2015).
- [6] I. I. Naumov, L. Bellaiche, and H. Fu, Unusual phase transitions in ferroelectric nanodisks and nanorods, *Nature* 432, 737 (2004).
- [7] A. K. Yadav, C. T. Nelson, S. L. Hsu, Z. Hong, J. D. Clarkson, C. M. Schlepütz, A. R. Damodaran, P. Shafer, E. Arenholz, L. R. Dedon, D. Chen, A. Vishwanath, A. M. Minor, L. Q. Chen, J. F. Scott, L. W. Martin, and R. Ramesh, Observation of polar vortices in oxide superlattices, *Nature* 530, 198 (2016).
- [8] A. Kholkin, A. Morozovska, D. Kiselev, I. Bdikin, B. Rodriguez, P. Wu, A. Bokov, Z.-G. Ye, B. Dkhil, L.-Q. Chen, M. Kosec, and S. V. Kalinin. Surface Domain Structures and Mesoscopic Phase Transition in Relaxor Ferroelectrics. *Adv. Func. Mat.* 21 (11), 1977 (2011).
- [9] G. Catalan, H. Béa, S. Fusil, M. Bibes, Patrycja Paruch, A. Barthélémy, and J. F. Scott, Fractal dimension and size scaling of domains in thin films of multiferroic BiFeO<sub>3</sub>, *Phys. Rev. Lett.* 100, 027602 (2008).
- [10] S. V. Kalinin, B. J. Rodriguez, J. D. Budai, S. Jesse, A. N. Morozovska, A. A. Bokov, and Z. G. Ye, Direct evidence of mesoscopic dynamic heterogeneities at the surfaces of ergodic ferroelectric relaxors, *Phys. Rev. B* 81, 064107 (2010).
- [11] V. V. Shvartsman, and A. L. Kholkin, Domain structure of (Pb (Mg<sub>1/3</sub>Nb<sub>2/3</sub>)O<sub>3</sub>)<sub>0.8</sub>(PbTiO<sub>3</sub>)<sub>0.2</sub> studied by piezoresponse force microscopy, *Phys. Rev. B* 69, 014102 (2004).
- [12] K. S. Wong, J. Y. Dai, X. Y. Zhao, and H. S. Luo, Time-and temperature-dependent domain evolutions in poled (111)-cut (Pb (Mg<sub>1/3</sub>Nb<sub>2/3</sub>)O<sub>3</sub>)<sub>0.7</sub> (PbTiO<sub>3</sub>)<sub>0.3</sub> single crystal, *Appl. Physics Lett.* 90, 162907 (2007).
- [13] A. N. Morozovska, E. A. Eliseev, J. Wang, G. S. Svechnikov, Yu. M. Vysochanskii, V. Gopalan, and L.-Q. Chen, Phase diagram and domain splitting in thin ferroelectric films with incommensurate phase, *Phys. Rev. B* 81, 195437 (2010).

- 
- [14] A. Artemev, B. Geddes, J. Slutsker, and A. Roytburd, Thermodynamic analysis and phase field modeling of domain structures in bilayer ferroelectric thin films, *J. Appl. Phys.* 103, 074104 (2008).
- [15] A. Hubert, and R. Schafer, *Magnetic domains: the analysis of magnetic microstructures*, Springer (1998).
- [16] D. Yadlovker, and S. Berger, Uniform orientation and size of ferroelectric domains, *Phys. Rev. B* 71, 184112 (2005).
- [17] D. Yadlovker, and S. Berger, Reversible electric field induced nonferroelectric to ferroelectric phase transition in single crystal nanorods of potassium nitrate, *Appl. Phys. Lett.* 91, 173104 (2007).
- [18] D. Yadlovker, S. Berger. Nucleation and growth of single crystals with uniform crystallographic orientation inside alumina nanopores. *J. Appl. Phys.* 101, 034304 (2007).
- [19] M. H. Frey, and D. A. Payne, Grain-size effect on structure and phase transformations for barium titanate, *Phys. Rev. B* 54, 3158 (1996).
- [20] Z. Zhao, V. Buscaglia, M. Viviani, M.T. Buscaglia, L. Mitoseriu, A. Testino, M. Nygren, M. Johnsson, and P. Nanni, Grain-size effects on the ferroelectric behavior of dense nanocrystalline BaTiO<sub>3</sub> ceramics, *Phys. Rev. B* 70, 024107 (2004).
- [21] A. V. Drobnich, A. A. Molnar, A. V. Gomonnai, Yu. M. Vysochanskii, and I. P. Prits, The effect of size factor on the phase transition in Sn<sub>2</sub>P<sub>2</sub>S<sub>6</sub> crystals: experimental data and simulation in ANNNI model, *Cond. Matt. Phys.* 6, 205 (2003)
- [22] E. Erdem, H.-Ch. Semmelhack, R. Bottcher, H. Rumpf, J. Banys, A. Matthes, H.-J. Glasel, D. Hirsch, E. Hartmann, Study of the tetragonal-to-cubic phase transition in PbTiO<sub>3</sub> nanopowders, *J. Phys.: Condens. Matter* 18, 3861–3874 (2006).
- [23] I. S. Golovina, V. P. Bryksa, V. V. Strelchuk, I. N. Geifman, and A. A. Andriiko, Size effects in the temperatures of phase transitions in KNbO<sub>3</sub> nanopowder, *J. Appl. Phys.* 113, 144103 (2013).
- [24] I. S. Golovina, V. P. Bryksa, V. V. Strelchuk, and I. N. Geifman, Phase transitions in the nanopowders KTa<sub>0.5</sub>Nb<sub>0.5</sub>O<sub>3</sub> studied by Raman spectroscopy. *Functional Materials.* 20, 75-80 (2013).
- [25] I. S. Golovina, B. D. Shanina, S. P. Kolesnik, I. N. Geifman, and A. A. Andriiko, Magnetic properties of nanocrystalline KNbO<sub>3</sub>, *J. Appl. Phys.* 114, 174106 (2013).
- [26] P. Perriat, J. C. Niepce, and G. Caboche. Thermodynamic considerations of the grain size dependency of material properties: a new approach to explain the variation of the dielectric permittivity of BaTiO<sub>3</sub> with grain size, *J. Therm. Anal. Calorim.* 41, 635 (1994).
- [27] H. Huang, C. Q. Sun, and P. Hing, Surface bond contraction and its effect on the nanometric sized lead zirconate titanate, *J. Phys.: Condens. Matter* 12, L127 (2000).
- [28] H. Huang, C. Q. Sun, Z. Tianshu, and P. Hing, Grain-size effect on ferroelectric Pb(Zr<sub>1-x</sub>Ti<sub>x</sub>)O<sub>3</sub> solid solutions induced by surface bond contraction, *Phys. Rev. B* 63, 184112 (2001).
- [29] M. Wenhui, Surface tension and Curie temperature in ferroelectric nanowires and nanodots, *Appl. Phys. A* 96, 915 (2009).
- [30] E. A. Eliseev, A.N. Morozovska, M.D. Glinchuk, and R. Blinc. Spontaneous flexoelectric/flexomagnetic effect in nanoferroics, *Phys. Rev. B* 79, 165433 (2009).

- 
- [31] A. N. Morozovska, E. A. Eliseev, and M.D. Glinchuk, Ferroelectricity enhancement in confined nanorods: Direct variational method, *Phys. Rev. B* 73, 214106 (2006).
- [32] A. N. Morozovska, M. D. Glinchuk, and E.A. Eliseev, Phase transitions induced by confinement of ferroic nanoparticles, *Phys. Rev. B* 76, 014102 (2007).
- [33] A. N. Morozovska, I. S. Golovina, S. V. Lemishko, A. A. Andriiko, S. A. Khainakov, and E. A. Eliseev. Effect of Vegard strains on the extrinsic size effects in ferroelectric nanoparticles, *Phys. Rev. B* 90, 214103 (2014).
- [34] J. Wang, A. K. Tagantsev, and N. Setter, Size effect in ferroelectrics: Competition between geometrical and crystalline symmetries, *Phys. Rev. B* 83, 014104 (2011).
- [35] E. A. Eliseev, A. V. Semchenko, Y. M. Fomichov, M. D. Glinchuk, V. V. Sidsky, V. V. Kolos, Yu. M. Pleskachevsky, M. V. Silibin, N. V. Morozovsky, and A. N. Morozovska, Surface and finite size effects impact on the phase diagrams, polar, and dielectric properties of (Sr, Bi)Ta<sub>2</sub>O<sub>9</sub> ferroelectric nanoparticles, *J. Appl. Phys.* 119, 204104 (2016).
- [36] V. V. Khist, E. A. Eliseev, M. D. Glinchuk, D. V. Karpinsky, M. V. Silibin, and A. N. Morozovska, Size effects of ferroelectric and magnetoelectric properties of semi-ellipsoidal bismuth ferrite nanoparticles, *J. Alloys Compd.* 714, 303 (2017)
- [37] C.-G. Duan, S.S. Jaswal, and E.Y. Tsymlal, Predicted magnetoelectric effect in Fe/BaTiO<sub>3</sub> multilayers: ferroelectric control of magnetism, *Phys. Rev. Lett.* 97, 047201 (2006).
- [38] G. Geneste, E. Bousquet, J. Junquera, and P. Ghosez, Finite-size effects in BaTiO<sub>3</sub> nanowires, *Appl. Phys. Lett.* 88, 112906 (2006).
- [39] M. Q. Cai, Y. Zheng, B. Wang, and G. W. Yang, Nanosize confinement induced enhancement of spontaneous polarization in a ferroelectric nanowire, *Appl. Phys. Lett.* 95, 232901 (2009).
- [40] J. W. Hong, G. Catalan, D. N. Fang, Emilio Artacho, and J. F. Scott, Topology of the polarization field in ferroelectric nanowires from first principles, *Phys. Rev. B* 81, 172101 (2010).
- [41] E. Bousquet, N. Spaldin, and Ph. Ghosez, Strain-induced ferroelectricity in simple rocksalt binary oxides, *Phys. Rev. Lett.* 104, 037601 (2010).
- [42] C.L. Wang, and S.R.P. Smith, Landau theory of the size-driven phase transition in ferroelectrics, *J. Phys.: Condens. Matter* 7, 7163 (1995).
- [43] A. N. Morozovska, E. A. Eliseev, R. Blinc, and M. D. Glinchuk, Analytical prediction of size-induced ferroelectricity in BaO nanowires under stress, *Phys. Rev. B* 81, 092101 (2010).
- [44] A. Sundaresan, R. Bhargavi, N. Rangarajan, U. Siddesh, and C.N.R. Rao, Ferromagnetism as a universal feature of nanoparticles of the otherwise nonmagnetic oxides, *Phys. Rev. B* 74, 161306(R) (2006).
- [45] D.D. Fong, G. B. Stephenson, S.K. Streiffer, J.A. Eastman, O.Auciello, P.H. Fuoss, and C. Thompson, Ferroelectricity in ultrathin perovskite films, *Science* 304, 1650 (2004).
- [46] J. Bardeen, Surface states and rectification at a metal semi-conductor contact, *Phys. Rev.* 71, 717 (1947).
- [47] V.M. Fridkin, *Ferroelectrics semiconductors*, Consultant Bureau, New-York and London (1980)



- 
- [48] M.A. Itskovsky, Some peculiarities of phase transition in thin layer ferroelectric, *Fiz. Tv. Tela* 16, 2065 (1974).
- [49] P.W.M. Blom, R.M. Wolf, J.F.M. Cillessen, and M.P.C.M. Krijn, Ferroelectric Schottky diode, *Phys. Rev. Lett.* 73, 2107 (1994).
- 50A.N. Morozovska, E.A. Eliseev, S.V. Svechnikov, A.D. Krutov, V.Y. Shur, A.Y. Borisevich, P. Maksymovych, and S.V. Kalinin. "Finite size and intrinsic field effect on the polar-active properties of ferroelectric semiconductor heterostructures." *Phys. Rev. B.* 81, 205308 (2010).
- [51] Y.A. Genenko, O. Hirsch, and P. Erhart, Surface potential at a ferroelectric grain due to asymmetric screening of depolarization fields, *J. Appl. Phys.* 115, 104102 (2014).
- [52] G.B. Stephenson, and M.J. Highland, Equilibrium and stability of polarization in ultrathin ferroelectric films with ionic surface compensation, *Phys. Rev. B* 84, 064107 (2011).
- [53] M. J. Highland, T. T. Fister, D. D. Fong, P. H. Fuoss, Carol Thompson, J. A. Eastman, S. K. Streiffer, and G. B. Stephenson, Equilibrium polarization of ultrathin  $\text{PbTiO}_3$  with surface compensation controlled by oxygen partial pressure, *Phys. Rev. Lett.* 107, 187602 (2011).
- [54] S. V. Kalinin, Y. Kim, D. Fong, and A. Morozovska, Surface screening mechanisms in ferroelectric thin films and its effect on polarization dynamics and domain structures, *Rep. Prog. Phys.* 81, 036502 (2018).
- [55] A. K. Tagantsev, and G. Gerra, Interface-induced phenomena in polarization response of ferroelectric thin films, *J. Appl. Phys.* 100, 051607 (2006).
- [56] Y. Gu, Menglei Li, A. N. Morozovska, Yi Wang, E. A. Eliseev, V. Gopalan, and L.-Q. Chen, Non-Ising character of a ferroelectric wall arises from a flexoelectric effect, *Phys. Rev. B* 89, 174111 (2014).
- [57] A. N. Morozovska, E. A. Eliseev, Y. A. Genenko, I. S. Vorotiahin, M. V. Silibin, Ye Cao, Y. Kim, M. D. Glinchuk, and S. V. Kalinin, Flexocoupling impact on the size effects of piezo-response and conductance in mixed-type ferroelectrics-semiconductors under applied pressure, *Phys. Rev. B* 94, 174101 (2016).
- [58] I. S. Vorotiahin, E. A. Eliseev, Qian Li, S. V. Kalinin, Yu. A. Genenko, and A. N. Morozovska, Tuning the polar states of ferroelectric films via surface charges and flexoelectricity, *Acta Mater.* 137, 85 (2017).
- [59] E. A. Eliseev, I. S. Vorotiahin, Y. M. Fomichov, M. D. Glinchuk, S. V. Kalinin, Yu. A. Genenko, and A. N. Morozovska, Defect driven flexo-chemical coupling in thin ferroelectric films, *Phys. Rev. B*, 97, 024102 (2018).
- [60] See Supplementary Materials, URL will be provided by Publisher
- [61] A. Belianinov, Q. He, A. Dziaugys, P. Maksymovych, E. Eliseev, A. Borisevich, A. Morozovska, J. Banys, Y. Vysochanskii, and S. V. Kalinin,  $\text{CuInP}_2\text{S}_6$  Room Temperature Layered Ferroelectric, *Nano Lett.* 15, 3808 (2015).
- [62] Note, that the coefficient  $g_{44}$  rules the polarization behavior, since this coefficient determines the energy of uncharged domain walls. Since  $g_{11}$  is not small and positive for CIPS (it is 5 times higher than  $g_{44}$ ) its influence appeared much less important even at the particle surface, and the next positive gradient terms add almost nothing to the physical picture we calculated. Also, we supposed isotropic properties in (001) plane,  $g_{44} = g_{55}$ .

- 
- [63] S.V. Kalinin, A.N. Morozovska, L.-Q. Chen, and B.J. Rodriguez, Local polarization dynamics in ferroelectric materials, *Rep. Prog. Phys.* 73, 056502 (2010).
- [64] Eugene A. Eliseev, Anna N. Morozovska, Sergei V. Kalinin, Yulan Li, Jie Shen, Maya D. Glinchuk, L.-Q. Chen, and V. Gopalan, Surface effect on domain wall width in ferroelectrics, *J. Appl. Phys.* 106, 084102 (2009).
- [65] A. Gruverman, O. Auciello, and H. Tokumoto, Imaging and control of domain structures in ferroelectric thin films via scanning force microscopy, *Annu. Rev. Mater. Sci.* 28, 101 (1998).
- [66] A. Gruverman, and A. Kholkin, Nanoscale ferroelectrics: processing, characterization and future trends, *Rep. Prog. Phys.* 69, 2443 (2006).
- [67] V. V. Shvartsman, and A. L. Kholkin, Evolution of nanodomains in  $0.9\text{PbMg}_{1/3}\text{Nb}_{2/3}\text{O}_3$ - $0.1\text{PbTiO}_3$  single crystals, *J. Appl. Phys.* 101, 064108 (2007).
- [68] S.V. Kalinin, A.N. Morozovska, L.-Q. Chen, and B. J. Rodriguez, Local polarization dynamics in ferroelectric materials, *Rep. Prog. Phys.* 73, 056502 (2010).